

## Subsurface Structure, Physical Properties, and Fault Zone Characteristics in the Scientific Drill Holes of Taiwan Chelungpu-Fault Drilling Project

Jih-Hao Hung<sup>1, \*</sup>, Yun-Hao Wu<sup>1</sup>, En-Chao Yeh<sup>2, 3</sup>, Jong-Chang Wu<sup>4, 5</sup>,  
and TCDP Scientific Party

(Manuscript received 27 October 2005, in final form 10 November 2006)

### ABSTRACT

Continuous coring and a suite of geophysical measurements were collected in two scientific holes to understand physical mechanisms involved in large displacements in the 1999 Chi-Chi earthquake. Physical properties of formations obtained from wire-line logs including P- and S-wave sonic velocity, gamma ray, electrical resistivity, density and temperature, are primarily dependent on parameters such as lithology, depth and fault zones. The average dip of bedding, identified from both cores and FMI (or FMS) logs, is about 30 degrees towards the SE. Nevertheless, local azimuthal variations and increasing or decreasing bedding dips appear across fault zones. A prominent increase in structural dip to 60° - 80° below 1856 m could be due to deformation associated with propagation of the Sanyi fault.

A total of 12 fault zones identified in Hole-A are located in the Plio-Pleistocene Cholan Formation, Pliocene Chinshui Shale and Miocene Kueichulin Formation. The shallowest fault zone at 1111 m in depth, FZ1111,

---

<sup>1</sup> Department of Earth Sciences and Institute of Geophysics, National Central University, Chung-Li, Taiwan, ROC

<sup>2</sup> Kochi Institute for Core Sample Research, Japan Agency for Marine-Earth Science and Technology, Kochi, Japan

<sup>3</sup> Department of Geosciences, National Taiwan University, Taipei, Taiwan, ROC

<sup>4</sup> Exploration and Development Research Institute, Chinese Petroleum Corporation, Miaoli, Taiwan, ROC

<sup>5</sup> Department of Earth Science, National Taiwan Normal University, Taipei, Taiwan, ROC

\* *Corresponding author address:* Prof. Jih-Hao Hung, Department of Earth Sciences and Institute of Geophysics, National Central University, Chung-Li, Taiwan, ROC; E-mail: jhhung@ncu.edu.tw

doi: 10.3319/TAO.2007.18.2.271(TCDP)

is a 1-m long gouge zone that includes 12-cm thick indurate black material and has been interpreted as the slip zone during Chi-Chi earthquake. FZ1111 is characterized by: 1) a bedding-parallel thrust fault with a 30-degree dip; 2) the lowest resistivity; 3) low density,  $V_p$  and  $V_s$ ; 4) high  $V_p/V_s$  ratio and Poisson's ratio; 5) low energy and velocity anisotropy, and low permeability or fluid mobility within the homogeneous gouge zone; 6) increasing gas ( $\text{CO}_2$  and  $\text{CH}_4$ ) emissions; and 7) being rich in smectite within the primary slip zone.

Formation physical properties hold consistent relationships with either depth or lithology. Anisotropy of shear-wave velocity shows that the dominant fast shear polarization direction is in good agreement with an overall azimuth of the maximum horizontal stress axis, particularly within the strong anisotropic Kueichulin Formation. A drastic change in orientation of fast shear polarization across the Sanyi thrust fault at a depth of 1710 m reflects changes in stratigraphy, physical properties and structural geometry.

(Key words: Chi-Chi earthquake, Taiwan Chelungpu-fault Drilling Project, Fault-zone fabrics, S-wave anisotropy)

## 1. INTRODUCTION

The 1999 Chi-Chi earthquake ( $M_w$  7.6) produced a 90-km long surface rupture zone along the north-south trending, west-vergent Chelungpu fault (CGS 2000; Fig. 1a). The most striking feature of the coseismic displacement field in the hanging-wall is that areas of large surface displacement lie above the footwall ramp of the thrust and at the northern termination. By contrast, relatively smaller, but significant (1 - 3 m) displacements are recorded at the footwall detachment (Yu et al. 2001; Dominguez et al. 2003; Lee et al. 2003). Along strike, both horizontal and vertical components of surface displacements increase from south to north and reach up to 12 m at the northern end near the Shihgang area. Surface ruptures indicate that the Chelungpu thrust runs parallel in map-view to the hanging-wall of the Pliocene Chinshui Shale indicating that the fault plane is a detachment in the Chinshui Shale.

In map-view (CPC 1982), south of Wufeng village, the Chelungpu fault merged with the Sanyi fault to the west into a single fault (Chang 1971; called Chelungpu-Sanyi fault hereafter) and emplaced the Pliocene Chinshui Shale on top of the Pleistocene Tokoushan Formation and Holocene deposits. The subsurface Chelungpu-Sanyi fault plane, imaged by both shallow and deep seismic profiling (Wang 2002; Wang et al. 2002a), shows a ramp-flat geometry as it slides along the base of the Chinshui Shale to the surface (Hung and Suppe 2002; Yue et al. 2005).

Towards the north, the Chelungpu-Sanyi fault branches into two segments (Fig. 1a): a) the underlying fault, called Sanyi thrust, which steps up from a deeper Pliocene and late-Miocene detachment in the Kueichulin and Tungkeng Formations and is probably not active, and b) the new North Chelungpu detachment (called Chelungpu fault hereafter) which is a

relatively young, nearly bedding-parallel fault in the Chinshui Shale and is the focus of some of the largest displacements in the Chi-Chi earthquake. Subsurface investigations of northern fault segments through a number of shallow seismic (Wang 2002; Wang et al. 2002b), deep petroleum seismic profiles (Hung and Wiltschko 1993) and shallow drilling (Huang et al. 2002; Tanaka et al. 2002; Hung and Liao 2003) confirm that the near-surface segment of Chelungpu thrust is parallel to both bedding and the underlying Sanyi fault to a depth of 3 km. The TCDP deep boreholes are drilled through this high-slip portion of the Chelungpu fault and through the Sanyi ramp in the footwall.

An important question that needs to be addressed is what physical properties or dynamic processes within the fault zone caused large coseismic displacements in the northern segment. Hypotheses that have been proposed include: 1) change of the fault-plane geometry; 2) static (long-term) physical properties such as an intrinsically low coefficient of friction, high pore-pressure and solution-transport chemical processes; and 3) dynamic change of physical properties during slip. A detailed look at the three-dimensional subsurface structure of the Chelungpu fault shows that surface coseismic displacements mimic the growth of active structures and geomorphology (Hung and Suppe 2002). Areas of large displacement in the north of the Chelungpu fault could be associated with a reduction of overburden as a result of the elevated Chelungpu ramp and flat (Yue et al. 2005).

The level of dynamic friction and stress during earthquake rupture is a key unknown (Zoback et al. 1987; Hickman 1991). If the coefficient of friction,  $\mu$ , follows Byerlee's Law and ranges from 0.6 to 0.9 (Byerlee 1978), frictionally generated heat should be observed near the Chelungpu fault zone (Mori 2003). On the other hand, the presence of clay-rich fault gouges (Wintsch et al. 1995; Vrolijk and van der Pluijm 1999; Warr and Cox 2001) and/or permanently high pore pressure (Hubbert and Rubey 1959; Suppe and Wittke 1977) within the fault zone can effectively reduce fault strength and the coefficient of friction (Tanaka et al. 2006). Other solution-transport mechanisms such as pressure solution and fluid-assisted mineral reactions may be important to determine the rheology of fault zones and the time scale of inter-seismic strength recovery (Blanpied et al. 1998; Rutter et al. 2001). The role of these mechanisms in determining the fault strength and earthquake instability mechanisms are unknown because of uncertainties regarding the mineralogy, microstructures and physical properties of fault zone materials and the nature and distribution of fluids at focal depths. Moreover, the "smooth" (low-level of high-frequency radiation) and "rapid" (high velocity) motion and large displacement in the north as opposed to larger accelerations and smaller displacements in the southern segment (Ma et al. 2000) may be attributable to the heterogeneity of fault rocks. The fault plane lies at the contact point of shale and conglomerate in the south but within the Chinshui Shale in the region of large displacements (Huang et al. 2002). In this regard, the physical properties of the fault-zone material and width and roughness of the fault zone probably vary considerably along the fault, and this heterogeneity may play an important role for the above mechanisms to operate during the rupture propagation (Tanaka et al. 2002; Heermance et al. 2003).

Contrary to high rock strength from both laboratory experiments and in-situ stress measurement, many dynamic weakening mechanisms (Mori et al. 2002) include slip weakening (Scholz 1998, 2002), thermal pressurization (Wibberley and Shimamoto 2005), mechani-

cal lubrication (Ma et al. 2003) and melting (Hirono et al. 2006). To differentiate this broad range of mechanisms requires knowledge of the physical properties of fault rocks, and heat flow and stress measurements before and after an earthquake. For example, physical examination of fault zone rocks could make it possible to infer important features such as deformation mechanisms of fault zone and dynamic frictional characteristics.

To address the above questions two holes (Hole-A and B) for Taiwan Chelungpu-fault Drilling Project (TCDP) were drilled during 2004 - 2005 at Dakeng, west-central Taiwan, where large surface slip (~10 m, M324 shown in Fig. 2) was observed. Subsurface structures were surveyed by reflection seismic method prior to the drilling (Wang et al. 2007). Continuous coring and geophysical down-hole logging for the two holes 40 meters apart were completed from a depth of 500 to 2003 m (Hole-A) and 950 to 1350 m (Hole-B), respectively. In this initial report we integrate results from cores, high-resolution micro-resistivity images of the borehole wall and wire-line down-hole geophysical logs to characterize subsurface structure, fault zones, and physical properties with measurements of cores, resistivity, density, gamma-ray, P- and S-wave velocity, and Formation MicroImager (FMI, mark of Schlumberger) and its predecessor, Formation MicroScanner (FMS) in Hole-A.

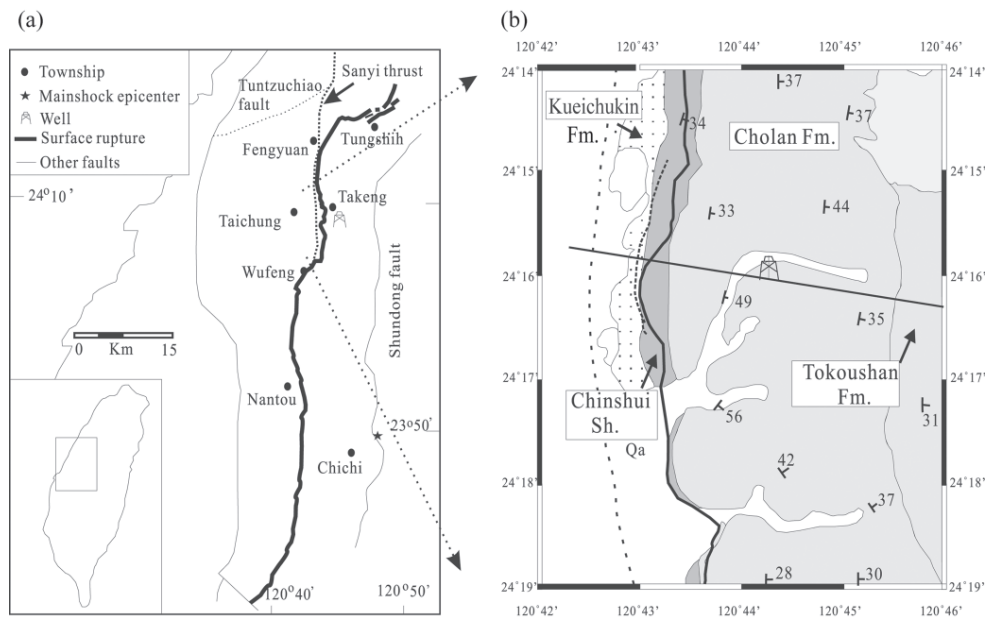


Fig. 1. (a) Locations of the epicenter of 1999 Chi-Chi main shock, surface ruptures (from CGS, 2000) and the Dakeng well. (b) A generalized geologic map (modified from the CPC 1982) showing stratigraphy near the drill site and the location of structural section. Note the rupture traces are confined within, but cut up and down the Chinshui Shale.

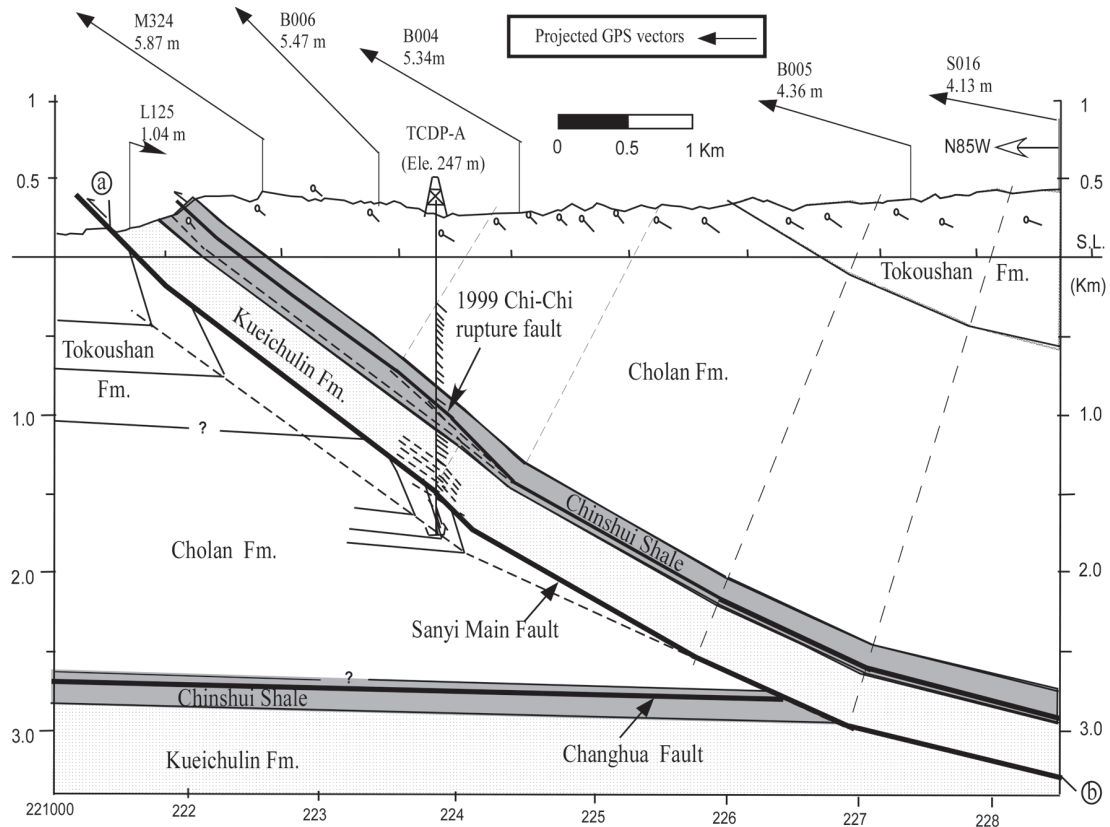
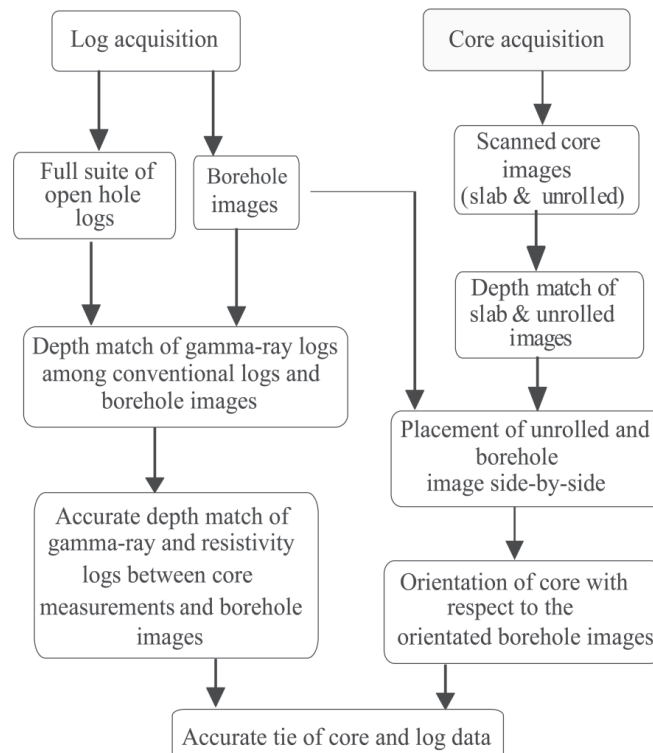


Fig. 2. Interpreted structural profile across the Dakeng well (Hole-A) based on the surface and subsurface drilled data. Measured depth intervals and true thickness (in parenthesis) of formations in this borehole include: Cholan, 0 - 1013 m (877 m); Chinshui, 1013 - 1300 m (249 m), and Kueichulin, 1300 - 1710 m (355 m). Locations of Chelungpu (Chi-Chi rupture), Sanyi and interpreted Changhua faults are shown by solid lines, and older faults formed prior to the Chi-Chi earthquake are shown by dashed lines. The displacement of the Sanyi fault is greater than 9 km (from the eroded base of the hanging-wall cutoff point “a” to footwall cutoff point “b”). The GPS vectors are projected components of the coseismic displacement in the plane of the section (station number and displacement are given; data from Yang et al. 2000). Note that the displacement vectors, except in the footwall of the rupture fault, are approximately parallel to the fault at depth.

## 2. CORE AND LOG INTEGRATION

Well log data are identified by wireline depths, whereas drilling depths are used in core data. A joint core and log study is important to calibrate the log data, extract particular subsurface physical information, and predict lithology at places where core recovery is incomplete (Lofts and Bristow 1998; Major et al. 1998).

We adopted a method of integration of core and log data via matching core with high resolution borehole images in the first step and then match the images with the log data in a second independent step (Fig. 3). The borehole image serves as a link between core-to-image and image-to-log integration procedures. Wireline log data collected from the Chinese Petroleum Corporation (CPC) and Schlumberger (SLB) and different logging runs must be free from depth mismatch. A common datum using derrick floor as a reference zero was applied to all logs. By correlating the total natural gamma-ray curves from the natural gamma-ray tool surveyed with each logging run, a depth shifting was imposed among logs of depth disparity caused by cable tension, tool sticking and different logging speed. The amounts of depth offset between the CPC and SLB increase with depth and range between 0.4 - 1.5 m.



*Fig. 3.* Flow chart summary of the strategy for core-log integration.

From the data sheet of the Drilling Information System (DIS) developed by the International Continental Scientific Drilling Program (ICDP), the core recovery rate is, on average, 92% for a total length of 1503 m. Cores of 8-cm diameter were wrapped in heat-shrinkage plastic tubes and then scanned with SmartCIS (camera image scanner) in both slab and unrolled modes at 300 dpi resolution and 24 bits color scale. This digital image resolution corresponds to 0.5 mm per pixel of actual core. A correlation between slab and unrolled core images has to be made since fractured cores cannot be scanned in an unrolled mode. The unrolled core images were then laid-out side-by-side with conventional logs and the borehole FMS/FMI images to produce a visual correlation between core and log data. Occasionally patches of cores have to be shifted a few meters at poorly recovered sections to match the FMI image and appropriate log depth. Both high core recovery rate and comparable vertical resolution between the core and borehole image (with 5-mm vertical resolution and nearly 100% and 50% coverage for FMI and FMS, respectively, in a borehole of 16-cm diameter) significantly reduce the depth match problem (Fig. 4). The FMI images serve as a link to correlate features in the core and log databases. The offset between the drilled and log-correlated depth varies within a limited range and usually accumulates with depth in each casing interval. In general, log depth is 0.4 to 2.2 m, 0.9 to 1.8 m, and 1.5 to 2 m, shallower than drilled depth in the three depth intervals of 500 - 1300 m, 1300 - 1750 m, and 1750 - 1870 m, respectively.

Cores were oriented by comparing core and borehole-wall images so that true dip azimuth and magnitudes can be calculated in both core and images. Geological interpretation and prediction of lithology can be also better addressed through the processes of core-to-image and image-to-log integration. The maximum depth of wire-line logging, depending on the borehole conditions, varies among tools in each run and ranges from 1750 to 1870 m. The FMI/FMS image tools are always logging first in each run and reach a maximum depth of 1870 m, below which only core data are available for analyses.

### 3. SUBSURFACE STRUCTURE AND FAULT ZONE CHARACTERISTICS

Surface geology (CPC 1982) near the drill site shows that surface ruptures of the Chi-Chi earthquake are confined within but cut up and down horizons of the Chinshui Shale (Fig. 1b). Formations encountered in Hole-A are mainly composed of clastic sedimentary rocks from Upper Miocene Kueichulin Formation to Pliocene Cholan Formation. Precise locations of formation boundaries were made by 1) correlating wireline logs among Hole-A and other nearby petroleum wells and 2) comparing stratigraphic sequences between surface outcrops and cores (Lin *et al.* 2007; Fig. 2). Cores below 1710 m consist of loose, under-compacted, gray-color siltstone to medium-coarse grained sandstone, and contain high fluid content shown by dense fluid drops trapped inside the surface of the plastic tubes. Characteristics of these sandstones are similar in lithology to surface exposed Cholan Formation. Reworked Miocene fossil, oyster beds at 1754 m and nanofossil assemblage zones of NN16 - 18 at 1714 m (Wu *et al.* 2007) also indicate that the footwall of the Sanyi fault is made up of repeated Cholan formation.

The main Chelungpu-Sanyi fault has accumulated a displacement of about 14 km along the main ramp and detachment at the location of the main-shock of the Chi-Chi earthquake (Yue *et al.* 2005). In the profile across the TCDP boreholes, the Sanyi thrust and Chelungpu



Regional bed attitude above 1710 m, identified from both cores and FMI/FMS images, is striking N15° - 21° E and dipping 20° - 40° (30° on average) toward the SE (Fig. 5). Nonetheless, intervals of increasing (from 30° to 75°) or decreasing (from 70° to 20°) dip magnitude as well as changes in dip azimuth appear across fault zones. A gradual increase of bedding dip with depth starts from FZ1710, and a drastic change of dip from 20° - 40° to 60° - 80° occurs across 1856 m where steep to overturned beds extend to the hole bottom.

A total of 13 distributed fault zones were identified exclusive of widely spaced, single shear fractures. The location and physical and structural features of each fault zone are listed in Tables 1 and 2. A general description and characterization of all fault zones were made by Yeh et al. (2007). The shallow 4 zones located in the Chinshui Shale. FZ1241 is a normal fault; the remaining three thrust faults can be categorized as part of the Chelungpu fault system. A detailed architecture of above fault zones was discussed in Sone et al. (2007). The 6 zones below this point are within the Kueichulin Formation and can be grouped as the Sanyi fault system. The main Sanyi thrust is encountered at 1710 m, where the Kueichulin Formation overlies the Cholan Formation.

Common fault rocks in the cores include intensely deformed fault core (clayey gouge) and adjacent highly fractured damage zones (fault breccia). The fault gouge is composed of ultra-fine grained clay minerals and massive to foliated fabrics; occasionally thin layers of indurate black material appear within the gouge zone. The paucity of veins inside the fault zones indicate that these fault rocks are formed in low temperature and by the fracturing process. Both microscopic observations of thin-sections and XRD analyses show that major mineral compositions are similar in both fault and host rocks (Isaacs et al 2007). FZ 1111 is bedding-parallel consisting of fault breccia and fault gouge 1109 to 1112 m. The degree of fracturing increases from the top of the damage zone towards the gouge zone in which the fabrics changed from massive to foliate between 1110.25 and 1111.35 m. The Chi-Chi major slip zone (MSZ, about 2 cm thick) is contained within the 12-cm thick primary slip zone (PSZ), which is located near the bottom of this broad gouge zone (Ma et al. 2006; Sone et al. 2007). FZ1710 is a major Sanyi fault zone that also contains about 1-m clayey gouge and a thrust fault type with nearly consistent bedding attitude in both the hanging- and footwalls (see Fig. 5).

#### 4. ROCK PHYSICAL PROPERTIES

A comprehensive suite of geophysical logs was collected from 500 to 1750 m. P- and S-wave sonic velocity, gamma ray, electrical resistivity, density and temperature were recorded at a 15-cm sampling interval (Fig. 6). Electrical image logs (FMS/FMI) are also acquired in the borehole to facilitate the analysis of fractures and faults intersected by the borehole. The hole-deviations are less than 4° above a depth of 1600 m but gradually increase downward to 14° at depth of 1865 m (see Fig. 6). Hole-drift was not measured below 1865 m but is believed to be greater than 14°.

Gamma ray radiation, formation resistivity, density and density-derived porosity are primarily dependent on the lithology. Variations in gamma ray radiation are associated with the presence of clay minerals. The gamma-ray log in sandstones of the Cholan Formation show a typical upward decreasing of radiation corresponding to an upward increase in both grain size

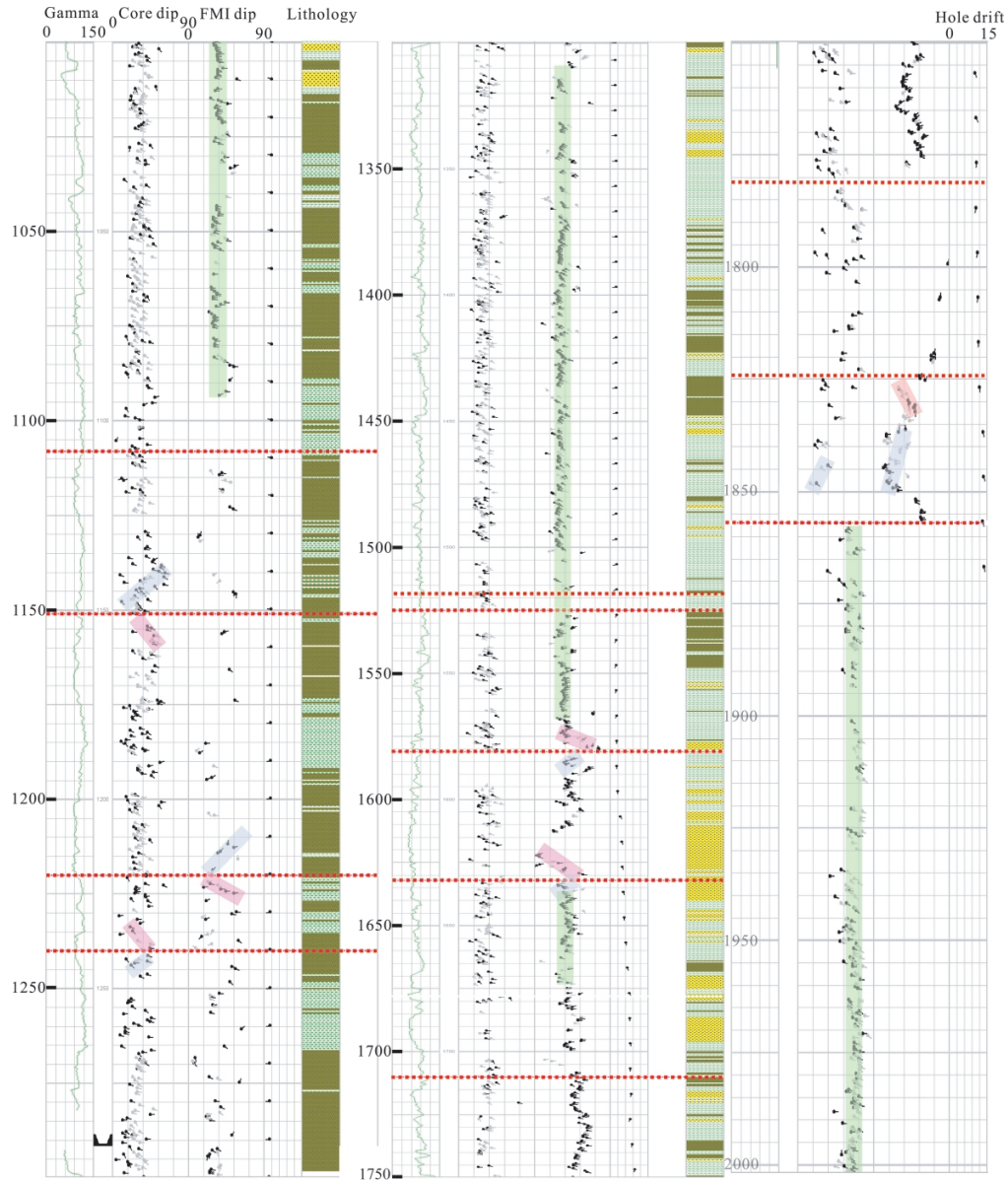


*Fig. 5.* Geometric relationship between fault zones and changes of bedding orientation derived from cores (second track) and FMI images (third track). The casing shoe is located at 1300 m, and the borehole drift is in the last track. The dip pattern across faults is shown by changes in dip magnitude (increase, “red pattern” and decrease, “blue pattern”) and dip azimuth (rotation or non-rotation) with depth, whereas strata exhibiting uniform orientation over a certain range are represented by a green pattern.

and sandstone/shale ratio in the core. Overall, sandstone has higher resistivity, higher porosity and lower density with respect to shale. Transient mud temperatures ( $\pm 10^{-3}$  °C) in the intervals 500 - 1275 m and 1275 - 1842 m show relatively low gradients of  $9^{\circ}\text{C km}^{-1}$  (40.0°C at 500 m to 46.8°C at 1275 m) and  $7^{\circ}\text{C km}^{-1}$  (50.4°C at 1275 m to 54.3°C at 1842 m), respectively. Although no thermal anomaly was observed due to circulation of mud immediately after the drilling, Kano et al. (2006) reported a slight heat signal around FZA1111 during repeated temperature measurements 6 months after the completion of drilling.

Velocity logs show an overall slight increase in both P- and S-wave sonic velocity with depths in the Cholan Formation (Fig. 6), but hold a constant value of  $3.99 \text{ km s}^{-1}$  ( $V_p$ ) and  $1.95 \text{ km s}^{-1}$  ( $V_s$ ) in the Chinshui Shale. Velocities increase again with depth in the Kueichulin Formation. Both P- and S-wave data show relatively low velocity in both sandstones and some fault zones with intense fracturing. The  $V_p/V_s$  ratio has an average value of 2.08 (equivalent to a Poisson's ratio,  $\nu$ , of 0.35) but can reach up to 2.4 ( $\nu = 0.4$ ) in the highly fractured fault zone. An abrupt change of physical properties occurred across FZ1710, below which values of resistivity, density and sonic velocities ( $V_p$  and  $V_s$ ) are significantly reduced by 50%, 3%, 18%, and 25%, respectively. The drastic change in physical properties provides independent evidence that

Table 1. Depth ranges (drilled depth) and core run number of 12 fault zones identified from cores. The fault zone is represented by the location of the fault core, and core depth (drilled) covers the entire damage zones. The top four fault zones within the Chinshui Shale are categorized as the Chelungpu fault system, below which the rest of the fault zones are located in the Kueichulin and underlying Cholan Formations and associated with the Sanyi thrust system.

Fault zone	Core Depth (m)	Run No.
FZA1111	1108.40 ~ 1111.20	R357 ~ R358
FZA1111	1108.40 ~ 1111.20	R357 ~ R358
FZA1153	1151.30 ~ 1153.92	R378 ~ R379
FZA1222	1220.50 ~ 1221.93	R426
FZA1241	1240.87 ~ 1241.86	R440
FZA1519	1518.80 ~ 1519.30	R562
FZA1525	1524.07 ~ 1527.64	R565 ~ R567
FZA1581	1581.20 ~ 1582.10	R588
FZA1632	1632.45 ~ 1633.00	R611
FZA1710	1711.80 ~ 1713.15	R652 ~ R653
FZA1785	1785.35 ~ 1785.65	R686
FZA1825	1824.57 ~ 1825.22	R702
FZA1855	1855.09 ~ 1856.29	R715

Table 2. Physical and structural features of fault zones from core and logging data (see text for explanation).

<b>Fault zone</b>	<b>Gouge Thickness (cm)</b>	<b>Color</b>	<b>Fluid content</b>	<b>Fault type</b>	<b>Lithology</b>	<b>Fault dip</b>	<b>Bed Dip Pattern</b>
FZA1111	60 - 100	LG	High	Thrust 105/30	Silt / Silt w/ Ss interbed	30	No drag No rotation
FZA1153	30 - 40	G	Low	Thrust 105/40	Silt w/ Ss interbed	40	Drag, No rotation Blue in HW Red in FW
FZA1222	5 - 10	G	Low	Thrust 015/28	Ss / Silt	28	No drag Rotation
FZA1241	5	BL	Dry	Normal 195/30	Silt / Silt	30	Drag, No rotation Red in HW Blue in FW
FZA1519	10	G	Med.	N/A	Silt / Ss	30	No drag No Rotation
FZA1525	15	G	Med.	Strike-slip 195/75	Ss / Ss	30	No drag Rotation
FZA1581	<1.5	G	High	Thrust 015/60	Mass. Ss / Ss	30	Drag, Rotation Red in HW Blue in FW
FZA1632	<0.5	G	Med.	N/A	Ss w / interbed Silt	30	Drag, Rotation Red in HW Blue in FW
FZA1710	85	G-DG	Med.	Thrust 105/30	Biot. Ss / layered Ss	30	No drag No rotation
FZA1785	20	DG	Low	N/A	Ss w / interbed sandy Silt	20	Drag, No rotation Red in HW Blue in FW
FZA1825	8	DG	Low	N/A	Ss w / interbed Silt	20	Drag, Rotation Red in HW Blue in FW
FZA1856	10	G	Med.	N/A	Silt. / Silt.	60	Drag, Rotation Blue in HW Red in FW

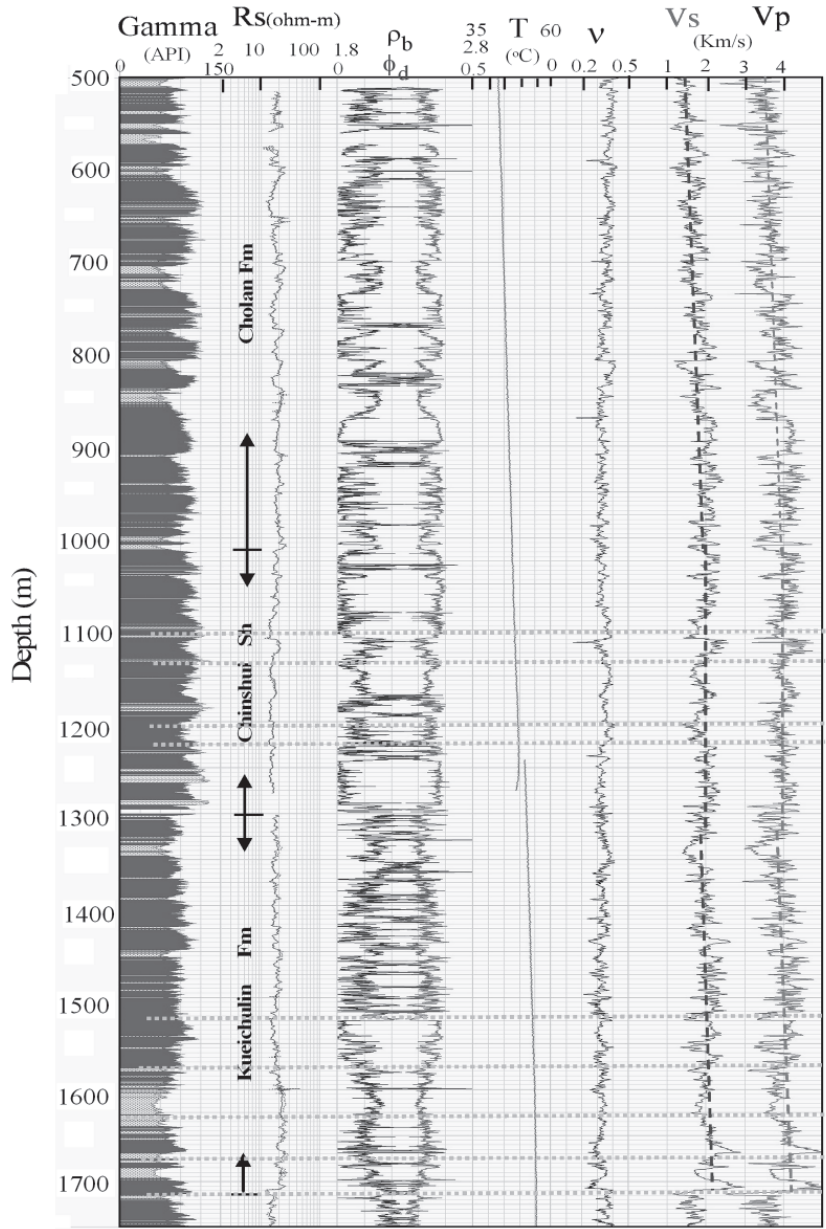


Fig. 6. Physical property logs in Hole-A between 500 and 1750 m. Track 1 is the lithology column determined from the Gamma-ray log. Other tracks from left to right include: resistivity, density and density derived porosity, temperature, Poisson ratio, shear- and p-wave velocities. Dashed lines on the sonic velocities indicate gross trends with depth. Locations of fault zones are marked in a dashed line.

FZ1710 is also a formation boundary. Most fault zones are characterized by relatively low resistivity and density, and high Poisson's ratio (Fig. 6). FZ1111 displays the following unique characteristics: 1) the breccia zone has the lowest resistivity value in the borehole, about 40% less than adjacent host rocks; 2) low density,  $V_p$  and  $V_s$  (20 - 25% reduction), but high  $V_p/V_s$  ratio (~2.4) and Poisson's ratio (~0.4); 3) low energy and velocity anisotropy, and fluid mobility (a proxy permeability) in the massive gouge zone (in DSI logs, see following section); 4) anomalously high discharge of formation gas (Yang et al. 2005).

## 5. SHEAR WAVE ANISOTROPY

Shear waves propagating through microcracks or planar fabrics can develop polarized orthogonal components of fast waves in the stiff direction and slow waves in the compliant direction that separate in time (Crampin and Lovell 1991). If the stress difference is large enough to close the cracks in one orientation, it is suitable to use shear-wave splitting to determine in-situ stress orientation. Data from Dipole Shear Sonic Imaging (DSI; mark of Schlumberger) logs acquired over an interval of 508 - 1870 m was used to assess shear wave velocity anisotropy. The DSI tool consists of monopole (P- and S-mode) and cross dipole sources at relatively low frequencies (0.8 - 5 kHz) and receiver arrays 15 cm apart (vertical resolution). The shear waves cause a flexing of the borehole wall which in turn excites shear waves penetrating approximately 1.5 m into the formation at a shear velocity of 1.5 km s<sup>-1</sup>. Three measurements of computed anisotropy- energy anisotropy, slowness anisotropy and time anisotropy- can be used to indicate the strength of anisotropy (Brie et al. 1998). Large energy differences between the maximum and minimum values of fast- and slow-shear waves, especially when minimum energy is low, indicate zones of significant anisotropy. Alternatively, other factors such as curved borehole trajectory and/or irregular borehole size that occur below 1750 m could also generate anomalous high minimum energy and cause an artifact in anisotropy.

Zones of significant anisotropy, with low minimum energy and difference between maximum and minimum energy over 50%, are prevalent in the Kueichulin Formation from the DSI log. Conversely, the energy difference, thickness and frequency of significant anisotropy are relatively less in the Cholan Formation (both the hanging-wall and footwall of the Sanyi thrust) than in both the Chinshui Shale and Kueichulin Formations. The overall uncertainty of fast shear azimuth is also related to the degree of shear anisotropy, which ranges between  $\pm 15^\circ$  and  $\pm 2^\circ$  in weak and strong anisotropic rocks, respectively. Results of analyses at the depth interval of 650 - 1850 m are shown by both scatter plots and rose diagrams of 8 discrete 150-m intervals of fast shear wave polarization (Fig. 7). Bedding trend and low-hemisphere stereo projection of fracture orientation are also shown at the same interval for comparison.

A prominent NW-SE fast shear polarizing direction was generally observed except in a few zones, such as 738 - 770, 785 - 815, 1517 - 1547, and 1700 - 1870 m, where dispersive orientations coupling with high minimum energy and low energy anisotropy appear. Particularly, a very consistent mean direction with small dispersion of  $115^\circ \pm 1^\circ \sim 2^\circ$  (95% confidence interval) appears in the strongly anisotropic Kueichulin Formation at 1300 - 1650 m. Relatively consistent fast shear polarization directions appear across FZ1111 (average  $165^\circ$  be-

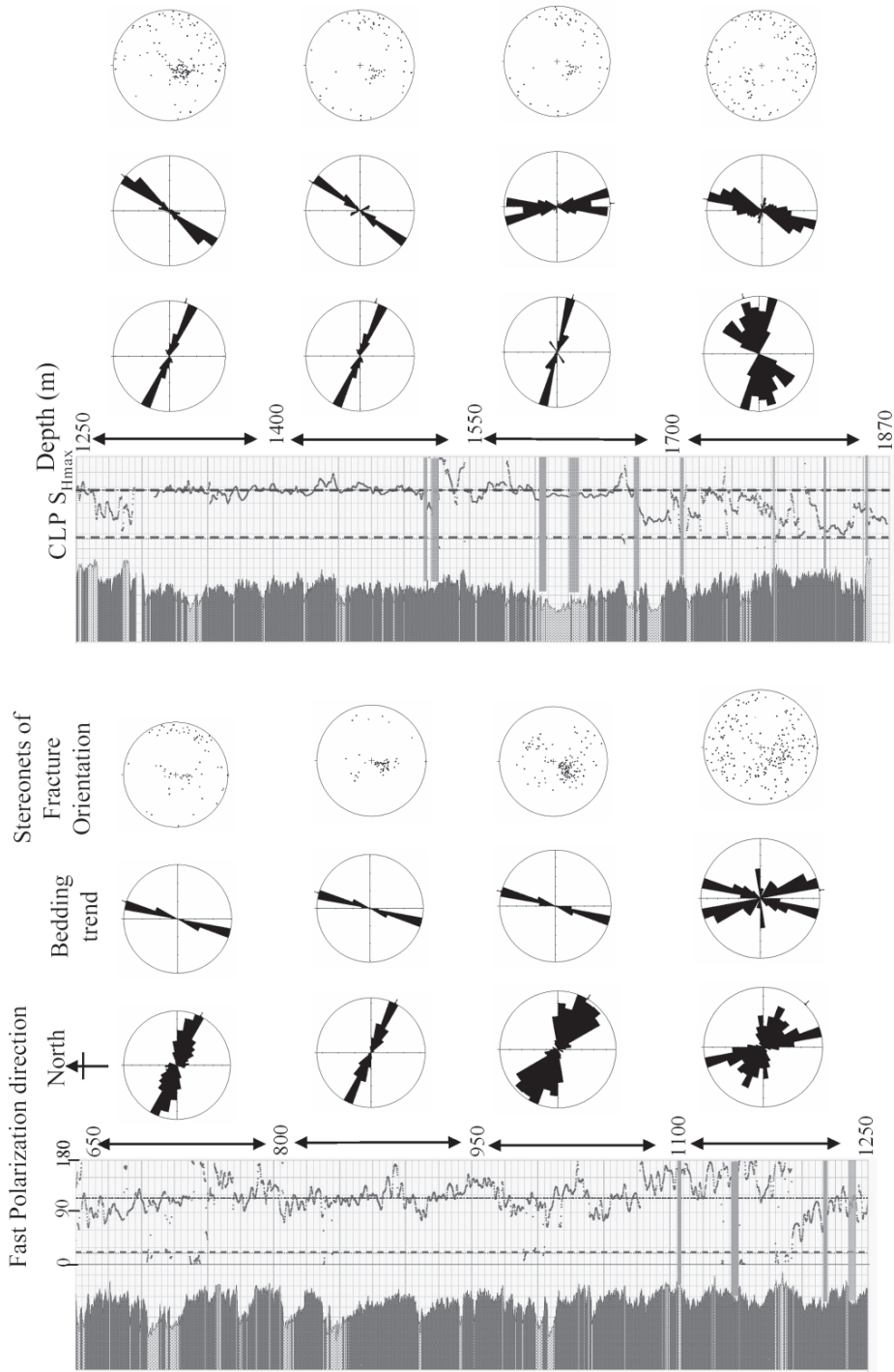


Fig. 7. Comparison of the fast-shear polarization direction with bedding trend determined from borehole images and fracture orientations measured from core images. Azimuths of the Chelungpu fault (CLF, 20°) and maximum horizontal principal stress ( $S_{Hmax}$ , 115°) determined from earthquake focal mechanisms in the central western foothills of Taiwan (Yeh et al. 1991) are shown for reference.

tween 1105 and 1115 m) compared to the interval of 1078 - 1190 m with trending in a much broader range of  $130^{\circ}$  -  $170^{\circ}$ . Thus, to the first order, there is no observable systematic change of trend in fast shear polarization across the Chi-Chi fault zone.

The overall NW-SE trending fast shear polarization is normal to subnormal to the bedding strike. Besides the predominant fast shear azimuth of  $115^{\circ}$ , other sub-directions occurred in averaging  $155^{\circ}$  and  $85^{\circ}$  (950 - 1250 m) and  $75^{\circ}$  (1700 - 1870 m). The two subsets of orientation  $155^{\circ}$  and  $85^{\circ}$  are geometrically formed as conjugates with respect to the main orientation of  $115^{\circ}$ . This mean direction of  $115^{\circ}$  is in good agreement with direction of regional maximum horizontal principal stress deduced from earthquake focal mechanisms by Yeh et al. (1991) in western central Taiwan.

## 6. DISCUSSION

We have characterized subsurface structure, fault zones and physical properties of formations in TCDP Hole-A through integrated studies of core and downhole geophysical measurements. In this section we provide interpretation on the origin of subsurface structure and the causes that could affect the anisotropy of shear wave velocity. Correlation between subsurface and surface mapped faults is also marked. Finally, we summarize the composite characteristics of the Chi-Chi rupture zone including fabrics, clay minerals, physical properties and thermal anomalies and their implications on the dynamic weakening mechanisms.

A drastic change of regional dip occurs across the Sanyi main thrust (FZ1710) from rather uniform to steep dip. The appearance of both steep to overturned beds and thrust faults underlying the Sanyi thrust (Fig. 2) is contrary to the observation of normal faults in the structural position 15 km to the north of the drill site (Hung and Wiltschko 1993, their Fig. 12). The extent of the contractional deformation beneath the Sanyi thrust is not known, nor is the boundary between the two structural styles. However, because the steep beds observed in the well do not crop out, the extent of the subthrust fold must be limited. We interpreted it as the overturned forelimb of a fault-propagation fold formed in front of the Sanyi thrust, later broken through along the anticlinal axial surface. Continued displacements along the Sanyi fault and surface erosion may annihilate the hanging-wall anticline and leave only the overturned footwall syncline. On the same line, the overturned beds are unlikely to have been produced by the underlying younger Changhua thrust in that movement along this fault would affect the entire structure above it.

We propose that thrust fault zones identified in the Chinshui Shale belong to the Chelungpu fault and that FZ1111 is the Chi-Chi rupture fault. These fault zones may merge together at depth (as shown in Fig. 2) from the observation that the Chelungpu-Sanyi fault is located near the base of the Chinshui shale. The Chi-Chi rupture fault could slip along the base of the Chelungpu fault at depth and/or cut up the section in the hanging-wall both along the strike and direction of transport (Chen and Ho 2000). A similar feature was also found in the subsurface drilling- the rupture fault is, in the TCDP drill hole, located near the top (FZ1111) in contrast to the bottom of the Chinshui Shale in the Fengyuan shallow hole towards the north (Huang et al. 2002; Tanaka et al. 2002). The Chelungpu and Sanyi faults are two separate fault

strands since the Sanyi fault cuts down stratigraphic section along-strike towards the north, whereas the Chelungpu fault becomes shallower towards north and east, and eventually merges with the eastern limb of the Cholan syncline where the Chi-Chi ruptures crops out at the surface north of the Taan Hsi.

The published geologic map (Ho and Chen 2000) of the Central Geologic Survey (CGS) in the Dakeng area is quite different from the previous CPC map (CPC 1982) in the following features: (1) a small tear or transfer fault cuts across the Dakeng River, and south of the fault the Chi-Chi surface ruptures lie within the Chinshui Shale and at the boundary between the mountain front and the Coastal Plain; (2) towards the north both structure salient and foothills are located farther west, and there is no surface exposure of the Chinshui Shale. If the CGS map is correct, the Chi-Chi rupture fault may locally cut up section from the Chinshui Shale at depth to the Cholan Formation at the surface (Lin et al. 2007). Regardless of the stratigraphy, an old, in-active fault located west of the Chi-Chi surface ruptures was mapped in the CPC geologic map (see Fig. 1b, dashed line) and by Lin et al. (2007) (his rupture-A fault). Both surface mapping and subsurface drilling showed a coherent result that the Chi-Chi rupture fault is a splay of the Chelungpu detachment fault and hinterlandward migration of splay faults (Fig. 2). Studies of terrace deformation around the Tachia River (Chen et al. 2003) infer the existence of an in-active fault (called Houli fault) between the Sanyi and the rupture-A faults. Despite that the Chinshui Shale is probably buried in the core of the small anticline associated with the rupture-A fault (Lin et al. 2007), the stratigraphic positions of both rupture-A and Houli faults are generally unknown since the bedrock was covered by terrace and alluvial deposits. Consequently, it is difficult to correlate above two faults with fault zones between FZ1111 and FZ1710 in TCDP-A hole.

There are several known causes of shear wave anisotropy in sedimentary rocks (Crampin and Lovell 1991; Esmersoy et al. 1995; Boness and Zoback 2004): 1) anisotropic in situ stresses that cause the preferred closure of fractures and generate a fast direction parallel to the regional maximum horizontal stress ( $S_{Hmax}$ ); 2) alignment of macrofractures without stress effects; 3) dilatancy of stress-aligned fluid-filled microcracks that produce the fast direction parallel to  $S_{Hmax}$ ; 4) alignment of minerals or grains; 5) anisotropy due to layering (bedding planes) in sedimentary rocks; and 6) borehole shape or azimuth of borehole ellipticity (Brie et al. 1998).

Because shear wave anisotropy displays a preferred orientation, observed random orientation of macroscopic fractures and faults (Fig. 7) cannot be the explanation. Alignment of mineral grains or fluid-filled dilatational microcracks is unlikely since no preferred orientations of minerals or veins are observed either on the cores or thin sections. Esmersoy et al. (1995) reported that there is little effect on shear anisotropy for vertical wells (or vertical propagation of shear waves) in layered beds with dip less than  $30^\circ - 40^\circ$ . A similar result was shown here that the strike of sedimentary beds or faults does not impose correlated effects since distinctly different directions between the fast shear wave and trend of the Chelungpu fault or beds has been observed. On the other hand, shear waves propagating through steep beds will split, and consequently, the NE-SW trend of fast shear polarization below 1710 m could be due to this effect. Other factors such as enlarged borehole size, irregular shape (rugosity) and deviated trajectory ( $8^\circ - 15^\circ$ ) may also contribute the azimuth dispersion of the fast shear wave in this depth range.

Consistent results appear in the cores and physical properties of fault zones. Among all fault zones, FZ1111 displays the lowest resistivity in the well, low density,  $V_p$  and  $V_s$ . The low resistivity is a result of infiltration of mud into highly fractured breccia based on core examination, and the low density,  $V_p$  and  $V_s$ , along with high  $V_p/V_s$  and Poisson's ratio in the gouge zone are attributable to large amounts of clay and/or fluid. Mineralogical analyses also show relatively high amounts of smectite and smectite/illite ratio in FZ1111 compared to other fault zones (Kuo et al. 2005; Song et al. 2007). Because smectite, upon heating, easily transforms into illite or smectite/illite mixed layers (Ho et al. 1999), the abundant smectite provides further evidence that FZ1111 was the slip zone during the Chi-Chi earthquake.

Despite large surface displacements, no temperature anomaly was observed and nearly hydrostatic fluid pressure was measured at FZ1111. Nevertheless, small positive amplitudes of heat anomaly were reported,  $0.1^\circ\text{C}$  in the shallow pilot hole (450 m deep) drilled near the Fengyuan city (Tanaka et al. 2006) and  $0.06^\circ\text{C}$  in Hole-A measured after the drilling (Kano et al. 2006). The small thermal anomalies indicate low frictional heat and low apparent (or dynamic) coefficients of friction,  $\mu = 0.12 \sim 0.13$  in the former and  $0.04 \sim 0.08$  in the latter. These values are extremely low compared to the static coefficient of friction determined in the laboratory, 0.6 to 0.7 (Byerlee 1978) or 0.35 to 0.5 for shale (Morrow et al. 1992). If the above estimates are applicable to the fault patch of large displacements, it indicates that dynamic mechanisms such as mechanical lubrication, frictional melting or thermal fluid pressurization could reduce the frictional strength. The small value of heat implies melting probably did not occur and explains why there were few microscopic textures of melting in the gouge layer. Furthermore, even if hydrostatic pressure was observed at the wellhead, without downhole in-situ measurement, it is difficult to evaluate if the over-pressurized pore pressure and/or mechanical weakening operated during the faulting process. Abnormally high pore pressure can be generated in frictional experiments using clay gouge in FZ1111 of low permeability between  $10^{-14}$  and  $10^{-17}$   $\text{m}^2$  (Sone et al. 2005). The high water content and smectite-rich clay gouge is suitable for mechanical weakening (Wu 1978; Chester et al. 1993; Wintsch et al. 1995) during faulting of the Chi-Chi earthquake.

## 7. CONCLUSIONS

Using cores and geophysical logs from TCDP Hole-A, we have characterized the subsurface structure, variations of physical properties with depth and the fault zone activated during the Chi-Chi earthquake. We find that P- and S-wave velocity and temperature in general increase with depth while gamma ray, resistivity, density and density-derived porosity are primarily dependent on the lithology. Among all fault zones, FZ1111 is the slip zone during the Chi-Chi earthquake and is characterized by anomalously low resistivity and density, and a high Poisson's ratio. A drastic change of physical properties across the Sanyi thrust fault at 1710 m, where the Kueichulin Formation is emplaced on top of the Cholan Formation. There is an excellent correlation between the fast polarization direction of shear wave and the maximum horizontal compression, particularly within the strong anisotropic Kueichulin Formation. Changes in the magnitude of shear-wave anisotropy and azimuth of fast shear polarizations below 1710 m are correlative with the change of stratigraphy, physical properties and structural geometry.

**Acknowledgements** We are grateful to Y. B. Tsai for initiating the drilling project and all participants of TCDP including project principal investigators, colleagues from JAMSTEC and several universities in Japan, and student assistants from NCU and NTU. We thank the International Continental Scientific Drilling Program (ICDP) for providing partial fund and technical consult. Thanks are also extended to two anonymous reviewers who help to improve this paper. This study was financially supported by the National Science Council, ROC under contract number of NSC93-2119-M-008-019 and NSC94-2119-M-008-009. This article is a TEC Contribution Number 00008.

## REFERENCES

- Blanpied, M. L., C. J. Marone, D. A. Lockner, J. D. Byerlee, and D. P. King, 1998: Quantitative measurement of the variation in fault rheology to fluid-rock interactions. *J. Geophys. Res.*, **103**, 9691-9712.
- Boness, N., and M. Zoback, 2004: Stress-induced seismic velocity anisotropy and physical properties in the SAFOD pilot hole in Parkfield, CA. *Geophys. Res. Lett.*, **31**, L15S17.
- Brie, A., T. Endo, and D. Hoyle, 1998: New directions in sonic logging. *Oilfield Review*, **10**, 40-55.
- Byerlee, J. D., 1978: Friction of rocks. *Pure Appl. Geophys.*, **116**, 615-629.
- CGS (Central Geological Survey), 2000: Report of Geological Investigation of 921 Chi-Chi Earthquake. Cent. Geol. Surv., MOEA, Taiwan, Taipei, ROC, 314 pp.
- Chang, S. L., 1971: Subsurface geologic study of the Taichung basin, Taiwan. *Petrol. Geol. Taiwan*, **8**, 21-45.
- Chen, M. M., and H. C. Ho, 2000: Correlation between Chi-Chi earthquake ruptures and the Chelungpu fault. *Spec. Publ. Cent. Geol. Surv.*, **12**, 113-138. (in Chinese)
- Chen, W. S., Y. G. Chen, R. C. Shih, T. K. Liu, N. W. Huang, C. C. Lin, S. H. Sung, and K. J. Lee, 2003: Thrust-related river terrace development in relation to the 1999 Chi-Chi earthquake rupture, Western Foothills, central Taiwan. *J. Asian Earth Sci.*, **21**, 473-480.
- Chester, F. M., J. P. Evans, and R. L. Biegel, 1993: Internal structure and weakening mechanisms of the San Andreas Fault. *J. Geophys. Res.*, **98**, 771-786.
- CPC (Chinese Petroleum Corporation), 1982: Geologic map of western Taiwan, Taichung sheet (1 : 100000). TPED, CPC, Miaoli, Taiwan.
- Crampin, S., and J. Lovell, 1991: A decade of shear-wave splitting in the Earth's crust: What does it mean? What use can we make of it? And what should we do next? *Geophys. J. Int.*, **107**, 387-407.
- Dominguez, S., J. P. Avouac, and R. Michel, 2003: Horizontal coseismic deformation of the 1999 Chi-Chi earthquake measured from Spot satellite images: Implications for the seismic cycle along the western foothills of central Taiwan. *J. Geophys. Res.*, **108**, 2083, doi: 10.1029/2001JB000951.
- Esmersoy, C., M. Kane, A. Boyd, and S. Denoo, 1995: Fracture and stress evaluation using dipole-shear anisotropy logs. *SPWL Symp. Trans.*, **36**, 12 pp.

- Heermance, R. V., Z. K. Shipton, and J. P. Evans, 2003: Fault structure control on fault slip and ground motion during the 1999 rupture of the Chelungpu fault. *Bull. Seismol. Soc. Am.*, **93**, 1034-1051.
- Hickman, S., 1991: Stress in the lithosphere and strength of active faults, US, Nat. Rep. Int. Union Geo. Geophys., 1987 - 1990. *Rev. Geophys.*, **29**, 759-775.
- Hirono, T., M. Ikehara, K. Otsuki, T. Mishima, M. Sakaguchi, W. Soh, M. Omori, W. Lin, E. Yeh, W. Tanikawa, and C. Y. Wang, 2006: Evidence of frictional melting from disk-shaped black material, discovered within the Taiwan Chelungpu fault system. *Geophys. Res. Lett.*, **33**, L19311, doi: 10.1029/2006GL027329.
- Ho, N. C., D. R. Peacor, and B. A. van der Pluijm, 1999: Preferred orientation of phyllosilicates in Gulf Coast mudstones and relation to the smectite-illite transition. *Clay Clay Miner.*, **47**, 495-504.
- Ho, H. C., and M. M. Chen, 2000: Explanatory text of the geological map of Taiwan, sheet 24: Taichung. Cent. Geol. Surv., Taipei, Taiwan, ROC.
- Huang, S. T., J. C. Wu, J. H. Hung, and H. Tanaka, 2002: Sedimentary facies, stratigraphy and deformation structures of cores from Fengyuan and Nantou wells of the Chelungpu fault. *Terr. Atmos. Ocean. Sci.*, **13**, 253-278.
- Hubbert, M. K., and W. W. Rubey, 1959: Role of fluid pressure in the mechanics of overthrust faulting. *Bull. Geol. Soc. Am.*, **70**, 115-166.
- Hung, J., and D. Wiltchko, 1993: Structure and kinematics of arcuate thrust faults in the Miaoli-Cholan area of western Taiwan. *Petrol. Geol. Taiwan*, **28**, 59-96.
- Hung, J., and J. Suppe, 2002: Subsurface geometry of the Sanyi-Chelungpu faults and fold scarp formation in the 1999 Chi-Chi Taiwan earthquake. *EOS Trans. AGU*, **83**, Fall Meeting Suppl., abstract T61B-1268.
- Hung, J., and C. F. Liao, 2003: Chelungpu fault drilling: deformation fabrics in the cores of the Fengyuan well. *Spec. Publ. Cent. Geol. Surv.*, **14**, 99-110. (in Chinese)
- Isaacs, A. J., J. P. Evans, S. R. Song, and P. T. Kolesar, 2007: Structural, mineralogical, and geochemical characterization of the Chelungpu thrust fault, Taiwan. *Terr. Atmos. Ocean. Sci.*, **18**, 183-221, doi: 10.3319/TAO.2007.18.2.183(TCDP).
- Kano, Y., J. Mori, R. Fujio, H. Ito, T. Yanagidani, S. Nakao, and K. Ma, 2006: Heat signature on the Chelungpu fault associated with the 1999 Chi-Chi, Taiwan earthquake. *Geophys. Res. Lett.*, **33**, L14306, doi: 10.1029/2006GL026733.
- Kuo, L., S. Song, and H. Chen, 2005: Characteristics of Clay Minerals in the Fault Zone of TCDP and its Implications. *EOS Trans. AGU*, **86**, Fall Meeting Suppl. abstract.
- Lee, Y. H., M. L. Hsieh, S. D. Lu, T. S. Shih, W. Y. Wu, Y. Sygyiyama, T. Azuma, and Y. Kariya, 2003: Slip vectors of the surface rupture of the 1999 Chi-Chi earthquake, western Taiwan. *J. Struct. Geol.*, **25**, 1917-1931.
- Lin, A. T., S. M. Wang, J. H. Hung, M. S. Wu, and C. S. Liu, 2007: Lithostratigraphy of the Taiwan Chelungpu-fault Drilling Project-A borehole and its neighboring region, central Taiwan. *Terr. Atmos. Ocean. Sci.*, **18**, 223-241, doi: 10.3319/TAO.2007.18.2.223 (TCDP).
- Lofts, J. C., and J. F. Bristow, 1998: Aspects of core-log integration: An approach using high resolution images. In: Harvey, P. K., and M. A. Lovell (Eds.), *Core-Log Integration*,

- Geol. Soc. London Spec. Publ., 136, 273-283.
- Ma, K. F., T. R. Song, S. J. Lee, and S. I. Wu, 2000: Spatial slip distribution of the September 20, 1999, Chi-Chi Taiwan earthquake inverted from teleseismic data. *Geophys. Res. Lett.*, **27**, 3417-3420.
- Ma, K. F., E. E. Brodsky, J. Mori, C. Ji, T. R. Song, and H. Kanamori, 2003: Evidence for fault lubrication during the 1999 Chi-Chi, Taiwan, earthquake ( $M_w$  7.6). *Geophys. Res. Lett.*, **30**, 1244, doi: 10.1029/2002GL015380.
- Ma, K. F., C. Y. Wang, J. H. Hung, S. R. Song, Y. B. Tsai, J. Mori, H. Tanaka, E. C. Yeh, H. Sone, L. W. Kuo, and H. Y. Wu, 2006: Slip zone and energetics of a large earthquake: Results from the Taiwan Chelungpu-fault Drilling Project. *Nature*, **444**, 473-476.
- Major, C. O., C. Pirmez, D. Goldberg, and Leg 166 Scientific party, 1998: High resolution core-log integration techniques: examples from the Ocean Drilling Program. In: Harvey, P. K., and M. A. Lovell (Eds.), *Core-Log Integration*, Geol. Soc. London Spec. Publ., 136, 85-29.
- Mitra, S., 1989: Fault-propagation folds: geometry, kinematic evolution, and hydrocarbon traps. *Am. Ass. Petrol. Geol.*, **74**, 921-945.
- Mori, J., H. Ito, and C. W. Wang, 2002: Chelungpu fault drilling could resolve seismological issues. *EOS Trans. AGU*, **83**, Fall Meeting Suppl., 255 pp.
- Mori, J., 2003: Source of processes of the 1999 Chi-Chi, Taiwan earthquake: Comparison to shallow faulting in subduction zones. *EOS Trans. AGU*, **84**, Fall Meeting Suppl. abstract T41-08.
- Morrow, C., B. Radlney, and J. D. Byerlee, 1992: Frictional strength and the effective pressure law of montmorillonite and illite clays. In: Brace, W. F., B. Evans, and T. F. Wong (Eds.), *Fault Mechanics and Transport Properties of Rocks*, Elsevier, New York, 69-89.
- Rutter, E. H., R. E. Holdsworth, and R. J. Knipe, 2001: The nature and tectonic significance of fault-zone weakening: an introduction. In: Holdsworth, R. E., R. E. Strachan, J. F. Magloughlin, and R. J. Knipe (Eds.), *The Nature and Tectonic Significance of Fault Zone Weakening*, Geol. Soc. London Spec. Publ., 186, 1-11.
- Scholz, C. H., 1998: Earthquakes and frictional laws. *Nature*, **391**, 37-42.
- Scholz, C. H., 2002: *The Mechanics of Earthquakes and Faulting*. Camb. Univ. Press, New York, 471 pp.
- Sone, H., T. Shimamoto, H. Noda, S. Song, K. Ma, J. Hung, and C. Wang, 2005: Frictional properties and permeability of fault rocks from Taiwan Chelungpu-fault Drilling Project and their implications for high-velocity slip weakening. *EOS Trans. AGU*, **86**, Fall Meeting Suppl. abstract, T43D-06.
- Sone, H., E. C. Yeh, T. Nakaya, J. H. Hung, K. F. Ma, C. Y. Wang, S. R. Song, and T. Shimamoto, 2007: Mesoscopic structural observations of cores from the Chelungpu Fault System, Taiwan Chelungpu-fault Drilling Project Hole-A, Taiwan. *Terr. Atmos. Ocean. Sci.*, **18**, 359-377, doi: 10.3319/TAO.2007.18.2.359(TCDP).
- Song, S. R., L. W. Kuo, E. C. Yeh, C. Y. Wang, J. H. Hung, and K. F. Ma, 2007: Characteristics of the lithology, fault-related rocks and fault zone structures in TCDP Hole-A. *Terr. Atmos. Ocean. Sci.*, **18**, 243-269, doi: 10.3319/TAO.2007.18.2.243(TCDP).

- Suppe, J., and J. H. Wittke, 1977: Abnormal pore-fluid pressures in relation to stratigraphy and structure in the active fold-and-thrust belt of northwestern Taiwan. *Petrol. Geol. Taiwan*, **14**, 11-24.
- Tanaka, H., C. Y. Wang, W. M. Chen, S. Arito, U. Kotaro, H. Ito, and A. Masataka, 2002: Initial science report of shallow drilling penetrating into the Chelungpu fault zone, Taiwan. *Terr. Atmos. Ocean. Sci.*, **13**, 227-251.
- Tanaka, H., W. M. Chen, C. Y. Wang, K. F. Ma, N. Urata, J. Mori, and M. Ando, 2006: Frictional heat from faulting of the 1999 Chi-Chi, Taiwan earthquake. *Geophys. Res. Lett.*, **33**, L163161029.
- Vrolijk, P., and B. A. van der Pluijm, 1999: Clay gouge. *J. Struct. Geol.*, **21**, 1039-1048.
- Wang, C. Y., 2002: The detection of a recent earthquake fault by the shallow reflection seismic method. *Geophysics*, **67**, 1345-1352.
- Wang, C. Y., C. L. Li, F. C. Su, M. T. Leu, M. S. Wu, S. H. Lai, and C. C. Chern, 2002a: Structural mapping of the 1999 Chi-Chi earthquake fault, Taiwan, by seismic reflection methods. *Terr. Atmos. Ocean. Sci.*, **13**, 211-226.
- Wang, C. Y., H. Tanaka, J. Chow, C. C. Chen, and J. H. Hung, 2002b: Shallow reflection seismics aiding geological drilling into the Chelungpu fault after 1999 Chi-Chi earthquake, Taiwan. *Terr. Atmos. Ocean. Sci.*, **13**, 153-170.
- Wang, C. Y., C. L. Lee, M. C. Wu, and M. L. Ger, 2007: Investigating the TCDP drill site using deep and shallow reflection seismics. *Terr. Atmos. Ocean. Sci.*, **18**, 129-141, doi: 10.3319/TAO.2007.18.2.129(TCDP).
- Warr, L. N., and S. Cox, 2001: Mineral transformations and weakening mechanisms along the Alpine Fault, New Zealand. In: Holdsworth, R. E., R. E. Strachan, J. F. Magloughlin, and R. J. Knipe (Eds.), *The Nature and Tectonic Significance of Fault Zone Weakening*, Geol. Soc. London Spec. Publ., 86, 85-101.
- Wibberley, C. A. J., and T. Shimamoto, 2005: Earthquake slip weakening and asperities explained by thermal pressurization. *Nature*, **436**, 689-692.
- Wintsch, R., R. Christoffersen, and A. Kronenberg, 1995: Fluid-rock reaction weakening of fault zones. *J. Geophys. Res.*, **100**, 13021-13032.
- Wu, J. C., S. T. Huang, M. H. Wang, C. C. Tsai, W. W. Mei, J. H. Hung, T. Y. Lee, K. M. Yang, and K. F. Lee, 2007: Core slabbing and nannofossil analysis on the Chelungpu fault zone, Taichung, Taiwan. *Terr. Atmos. Ocean. Sci.*, **18**, 295-325, doi: 10.3319/TAO.2007.18.2.295(TCDP).
- Wu, F. T., 1978: Mineralogy and physical nature of clay gouge. *Pure Appl. Geophys.*, **116**, 655-689.
- Yeh, E. C., H. Sone, T. Nakaya, K. H. Ian, S. R. Song, J. H. Hung, W. Lin, T. Hirono, C. Y. Wang, K. F. Ma, W. Soh, and M. Kinoshita, 2007: Core description and characteristics of fault zones from Hole-A of the Taiwan Chelungpu-fault Drilling Project. *Terr. Atmos. Ocean. Sci.*, **18**, 327-357, doi: 10.3319/TAO.2007.18.2.327(TCDP).
- Yeh, Y. H., C. H. Lin, E. Barrier, and J. Angelir, 1991: Stress tensor analysis in the Taiwan area from focal mechanisms of earthquake. *Tectonophysics*, **200**, 267-280.
- Yang, T., V. Walia, H. Lee, S. Song, and C. Wang, 2005: Compositions of on-site monitoring on dissolved gas of drilling mud flow and pore-gases of drilled cores of TCDP. *EOS*

- Trans. AGU*, **86**, Fall meeting suppl., abstract T51A-1315.
- Yang, M., R. J. Rau, J. Y. Yu, and T. T. Yu, 2000: Geodetically observed surface displacements of the 1999 Chi-Chi, Taiwan, earthquake. *Earth Planet. Space*, **52**, 403-413.
- Yu, S. B., L. C. Kuo, Y. J. Hsu, H. H. Su, and C. C. Liu, 2001: Preseismic deformation and coseismic displacements associated with the 1999 Chi-Chi, Taiwan, earthquake. *Bull. Seismol. Soc. Am.*, **91**, 995-1012.
- Yue, L. F., J. Suppe, and J. Hung, 2005: Structural geology of a classic thrust belt earthquake: The 1999 Chi-Chi earthquake Taiwan ( $M_w = 7.6$ ). *J. Struct. Geol.*, **27**, 2058-2083.
- Zoback, M., M. L. Zoback, V. S. Mount, J. Suppe, J. P. Eaton, J. H. Healy, D. Oppenheimer, P. Reasenber, L. Jones, C. B. Raleigh, I. G. Wong, O. Scotti, and C. Wentworth, 1987: New evidence on the state of stress of the San Andreas fault system. *Science*, **238**, 1105-1111.
- 
- Hung, J. H., Y. H. Wu, E. C. Yeh, J. C. Wu, and TCDP Scientific Party, 2007: Subsurface structure, physical properties, and fault zone characteristics in the scientific drill holes of Taiwan Chelungpu-fault Drilling Project. *Terr. Atmos. Ocean. Sci.*, **18**, 271-293, doi: 10.3319/TAO.2007.18.2.271(TCDP).